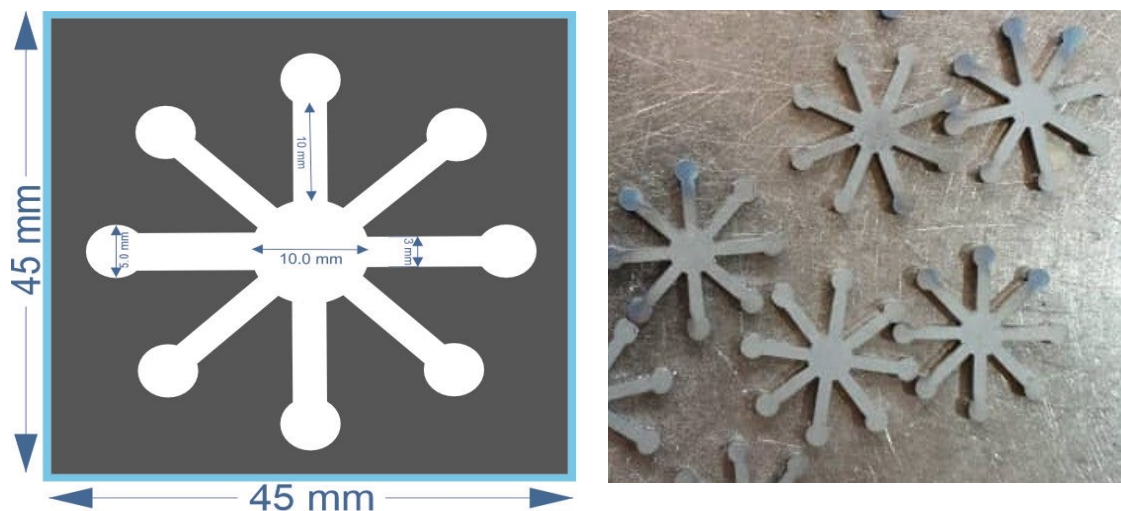


Supporting Information

Smartphone-assisted microfluidic and spectrophotometric recognition of hydrazine: A new platform towards rapid analysis of carcinogenic agents and environmental technology

Kambiz Ghaseminasab ^a, Nastaran Aletaha ^b, Mohammad Hasanzadeh ^{b,c,d}



Scheme. S1. A) Pattern designed by the AutoCAD software to make a stainless-steel mold with dimensions' d = 5 mm for the peripheral circles, d = 10 mm for the central circle, 10 mm for the length of the channels, and 3 mm meters for the width of the channels. **B)** Photographic Images of fabricated steel patterns.

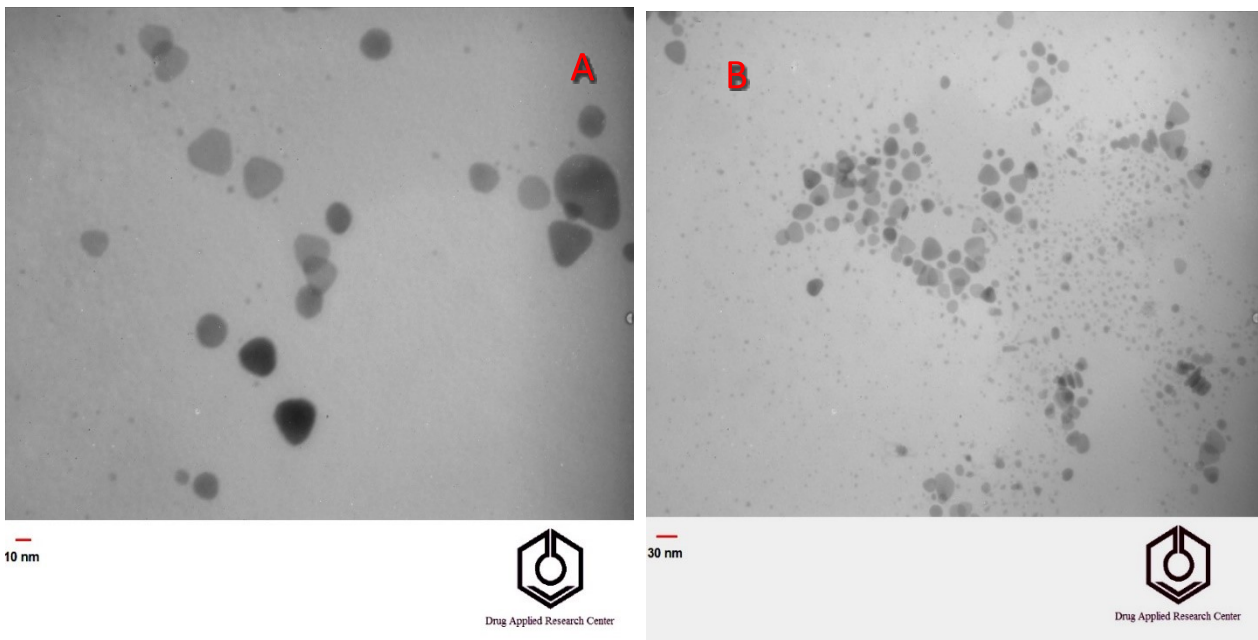


Fig. S1. TEM images of Ag NPrs in different magnification 10 nm **A)** and 30 nm **B)**

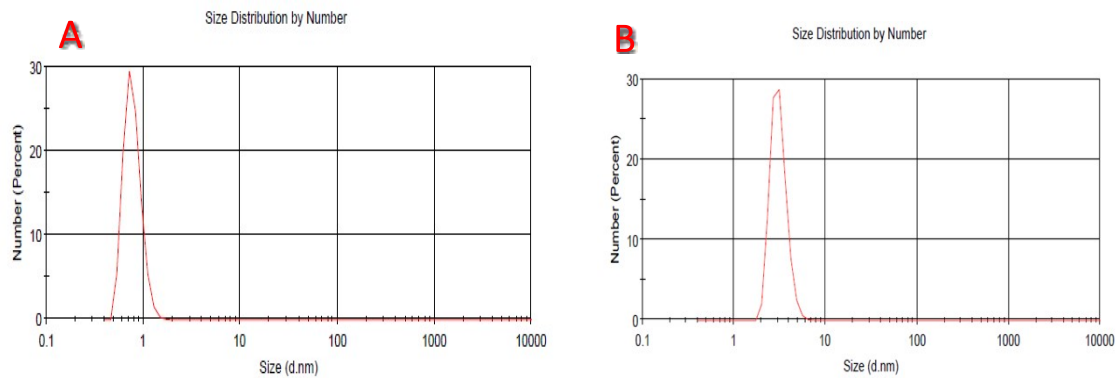


Fig. S2. DLS plot of: **A)** Ag NPrs, **B)** combination of Ag NPrs and Hyd (immediately, t = 0s)

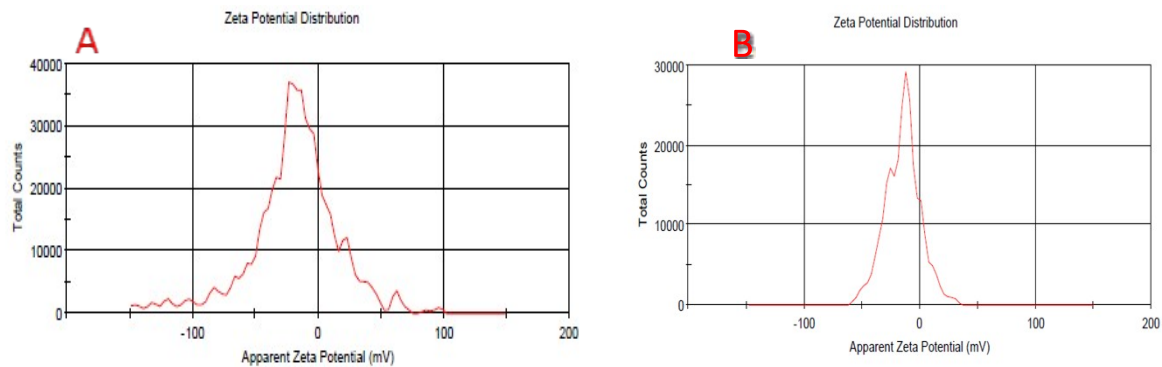


Fig. S3. Zeta potential of **A)** Ag NPrs, **B)** combination of Ag NPrs and Hyd (immediately, t = 0s)

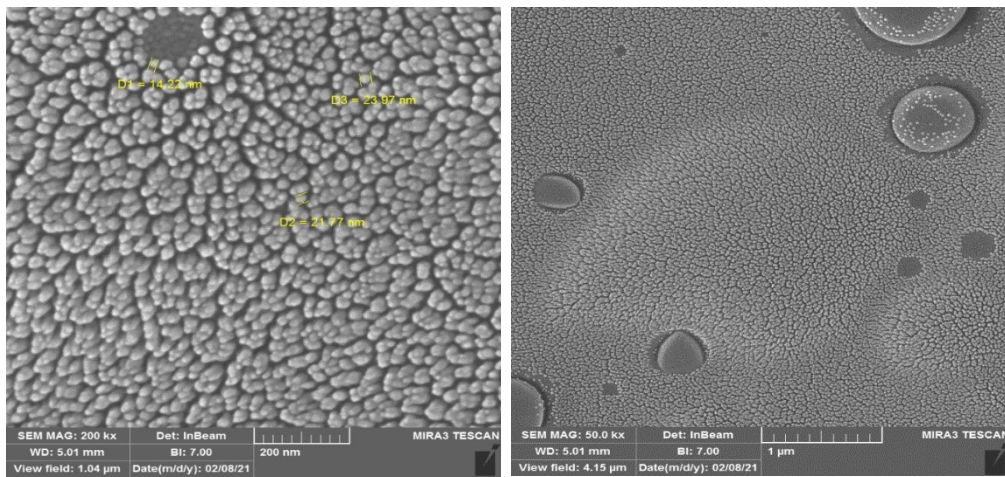


Fig. S4. FE-SEM images of Ag NPrs in different magnification.

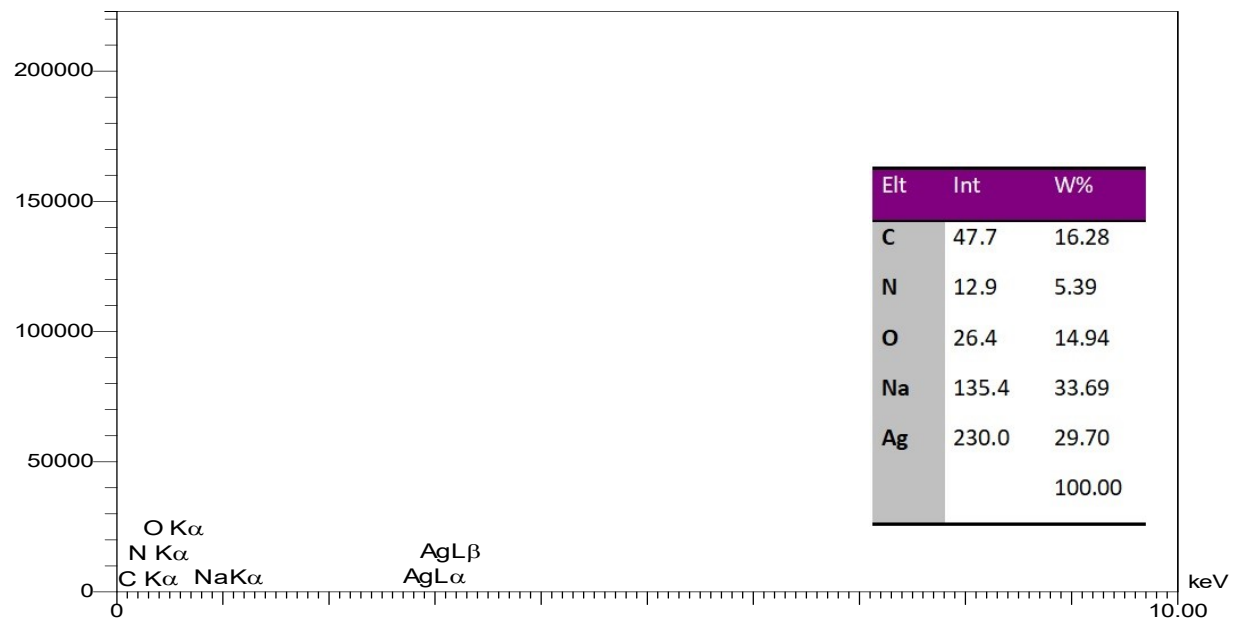


Fig. S5. EDS spectra of Ag NPrs.

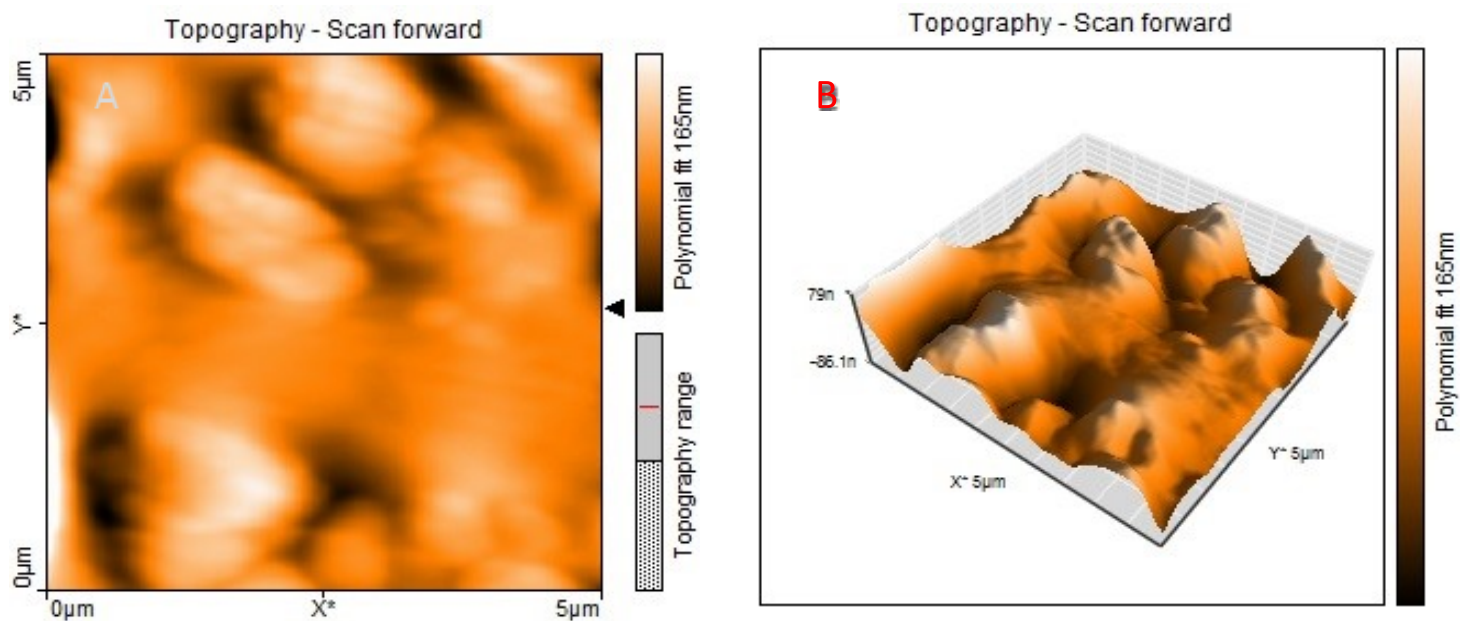


Fig. S6. Topographic AFM images of Ag NPrs in 2D, (A) and 3D, (B) view.

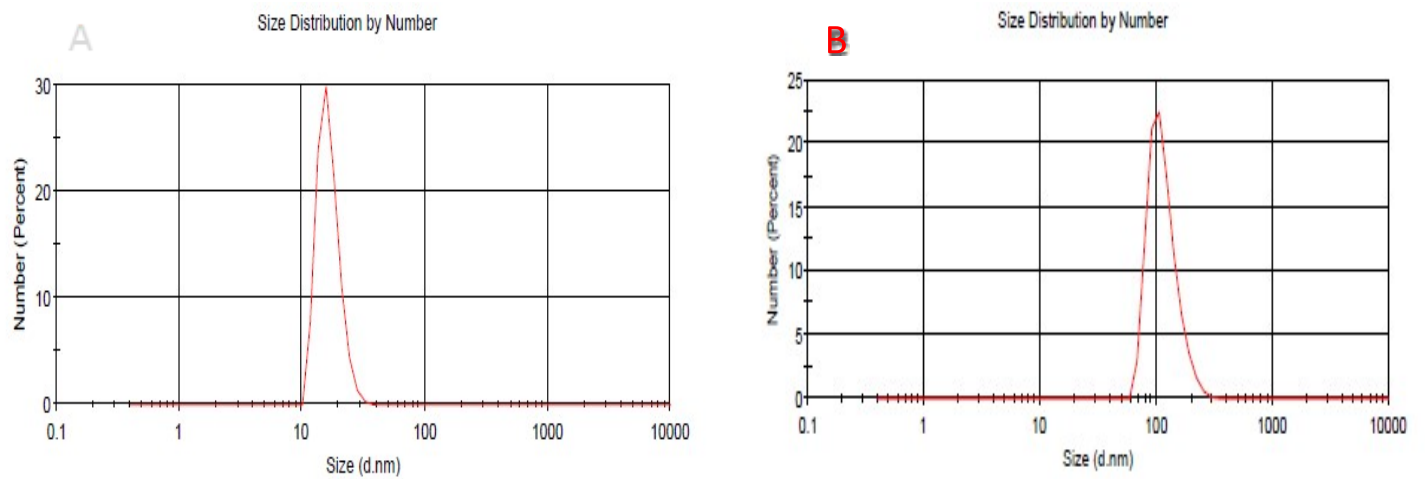


Fig. S7. DLS plot of **A)** Ag NWs, **B)** combination of Ag NWrs and Hyd (immediately, $t = 0\text{s}$)

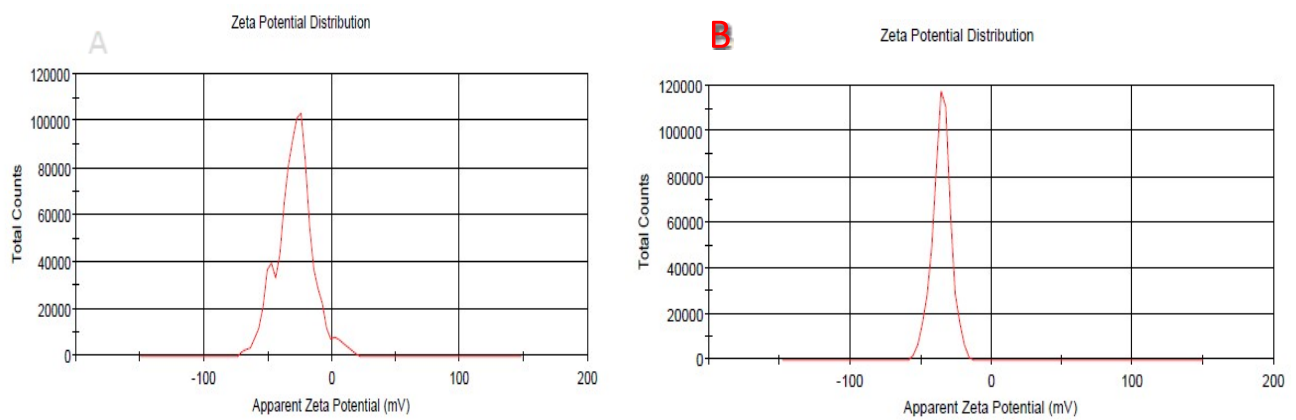


Fig. S8. Zeta potential of **(A)** Ag NWs, **(B)** combination of Ag NWs and Hyd (immediately, $t = 0\text{s}$)

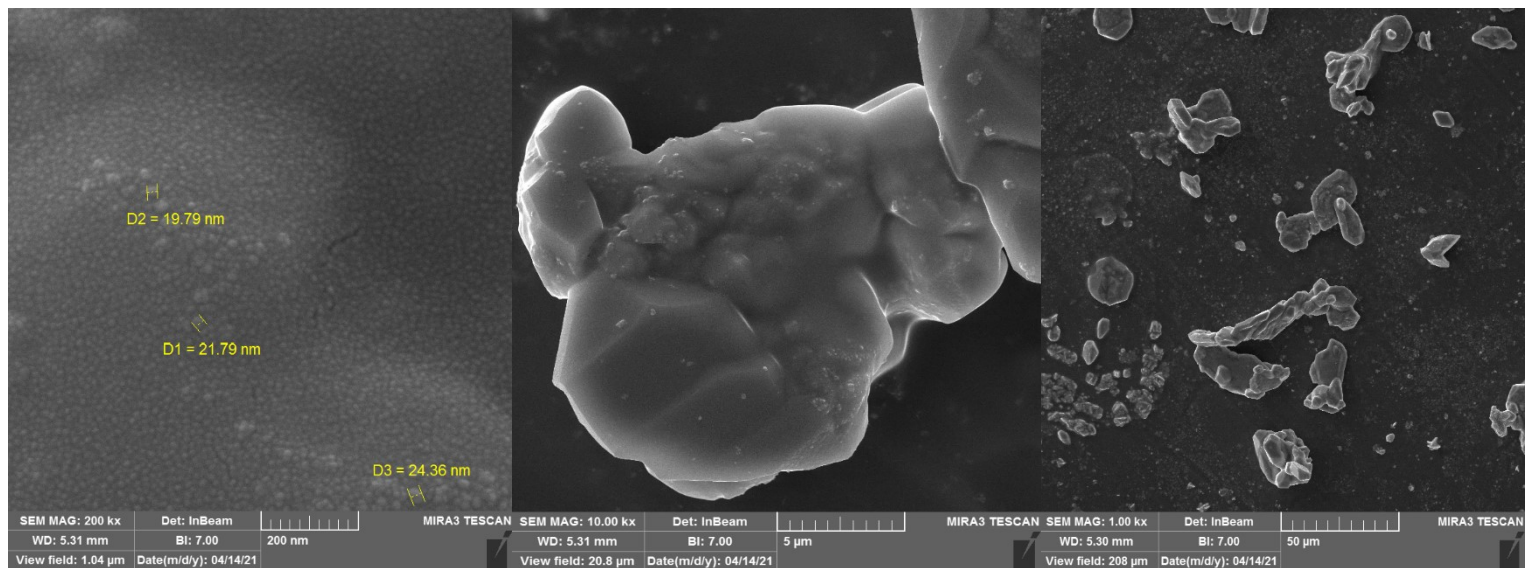


Fig. S9. FE-SEM images of Ag NWs in different magnification.

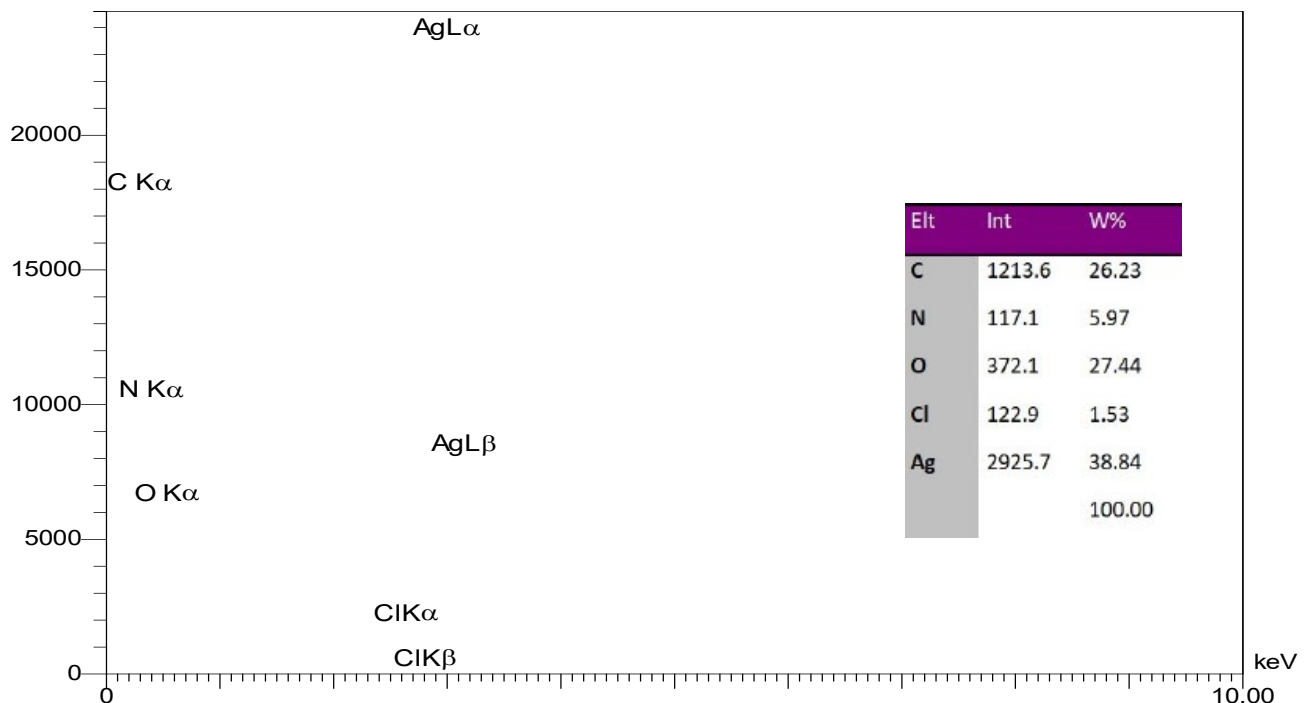


Fig. S10. EDS spectra of Ag NWs.

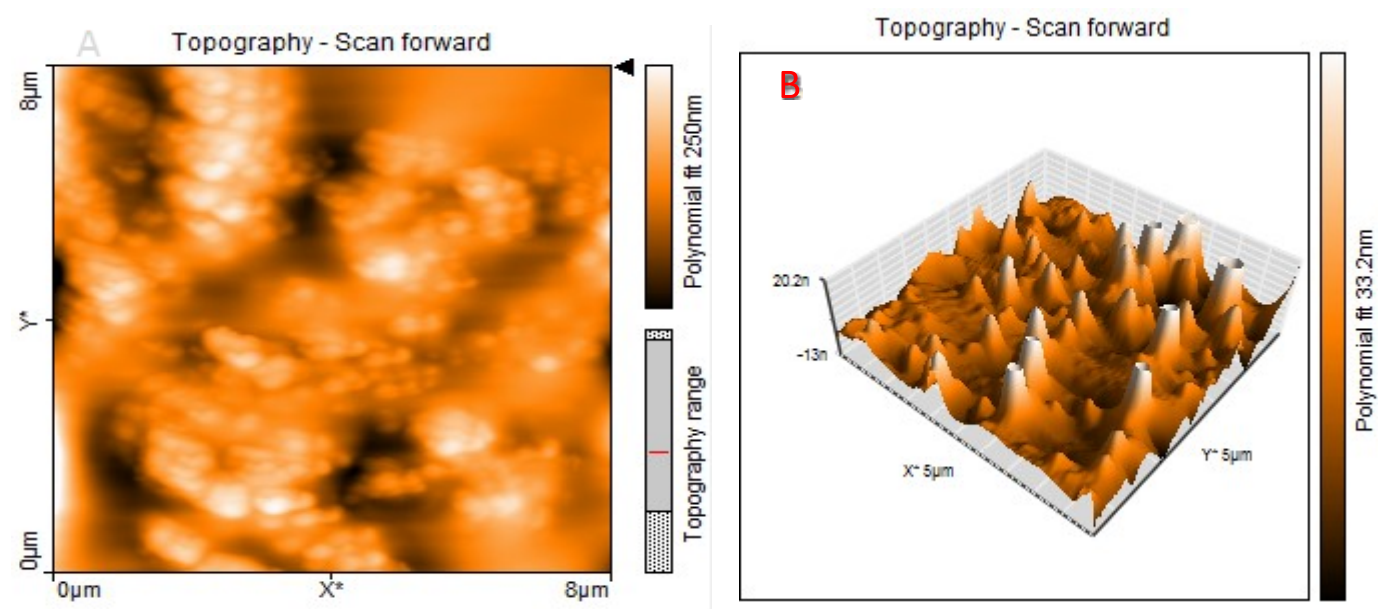


Fig. S11. Topographic AFM images in 2D, **(A)** and 3D, **(B)** view of Ag NWs.

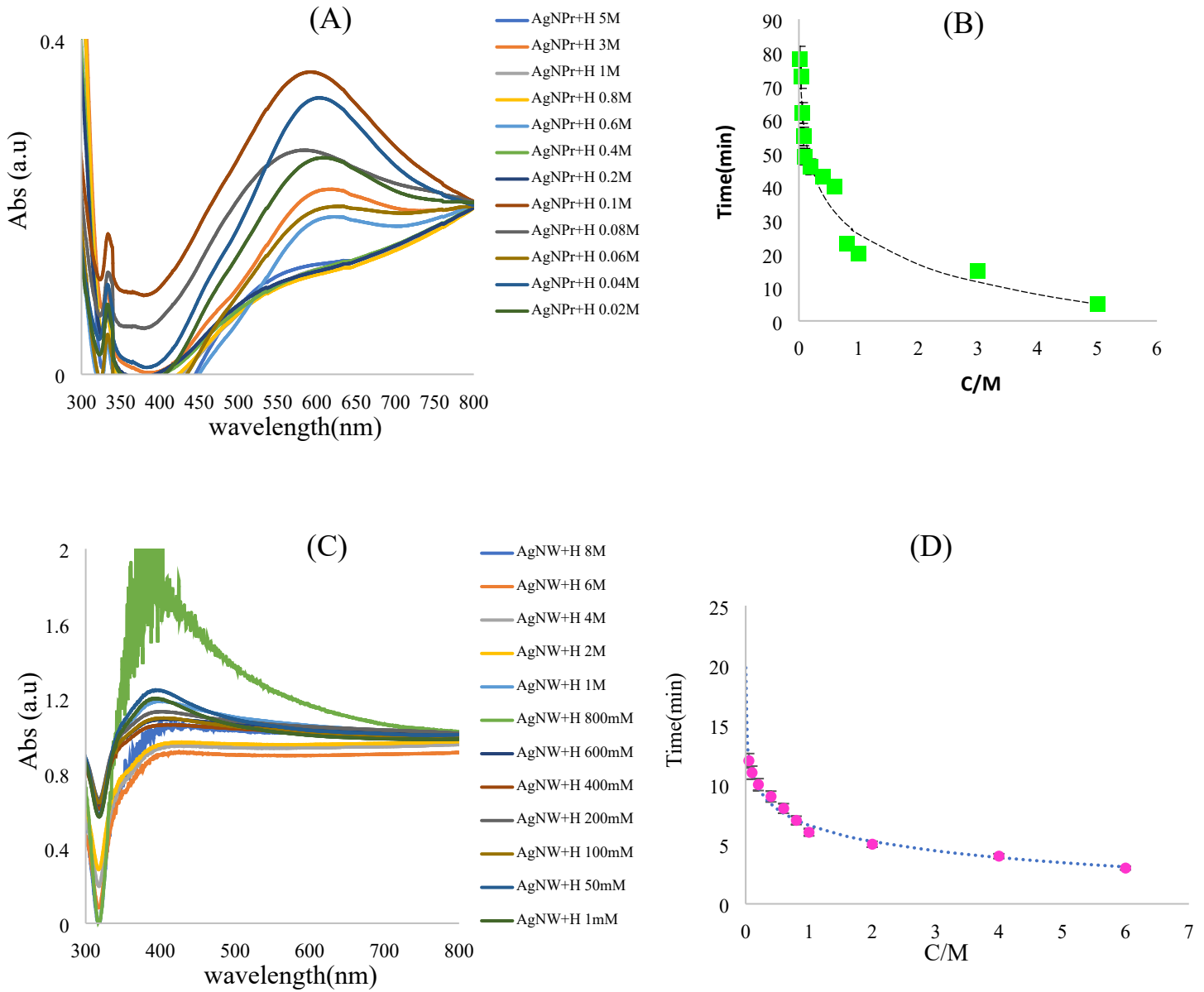
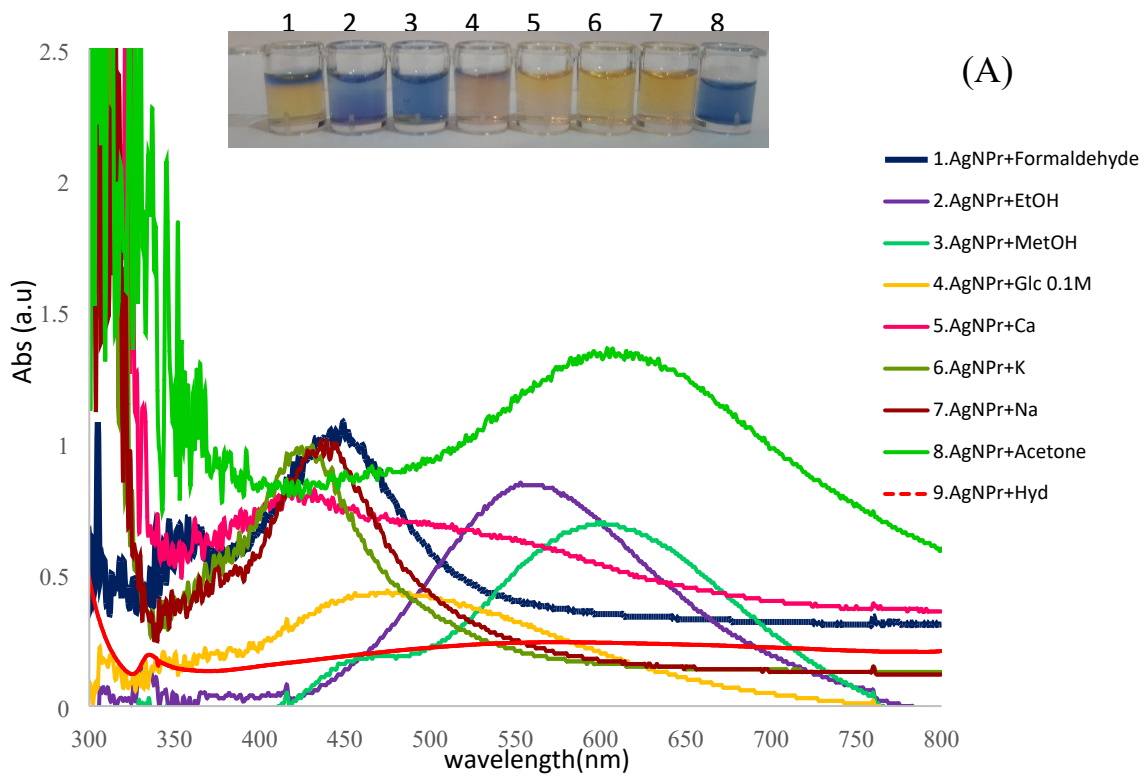
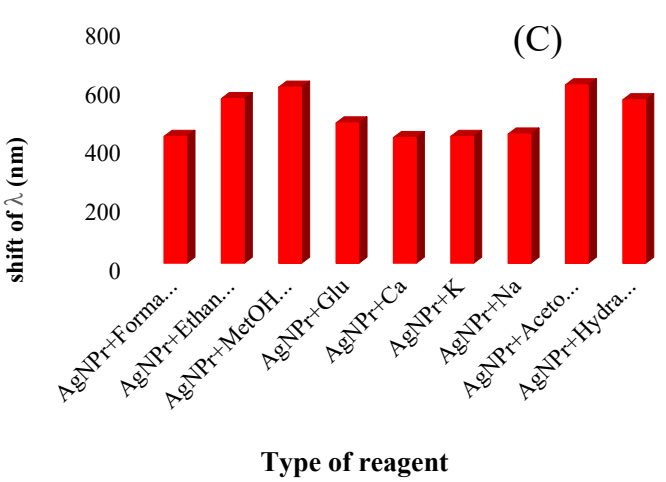
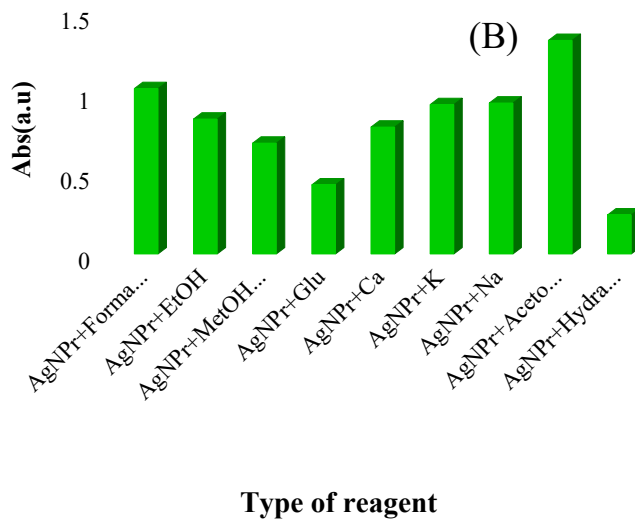
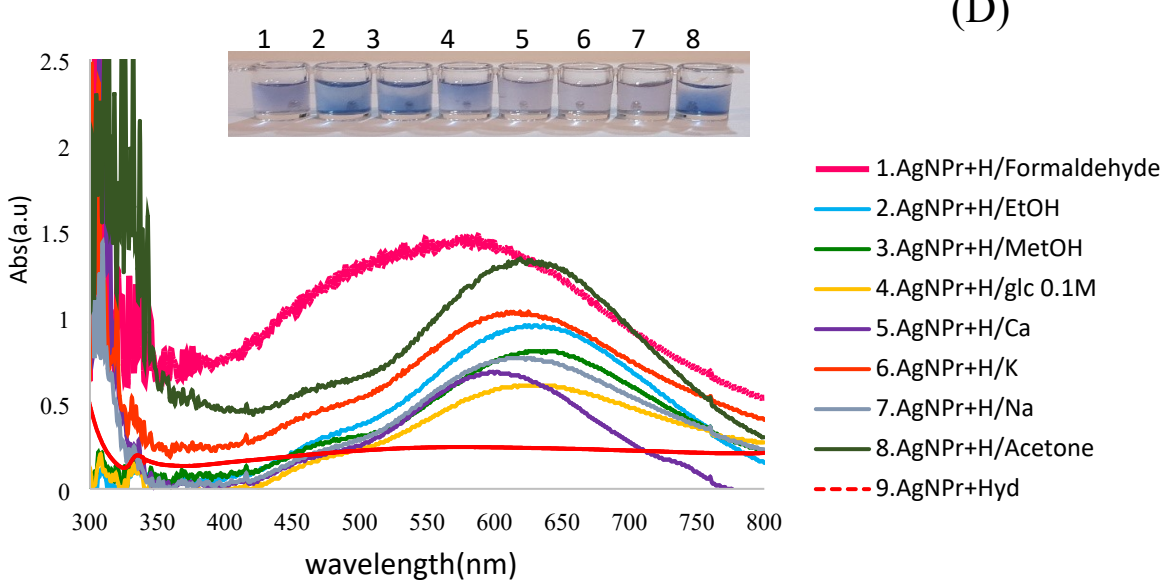
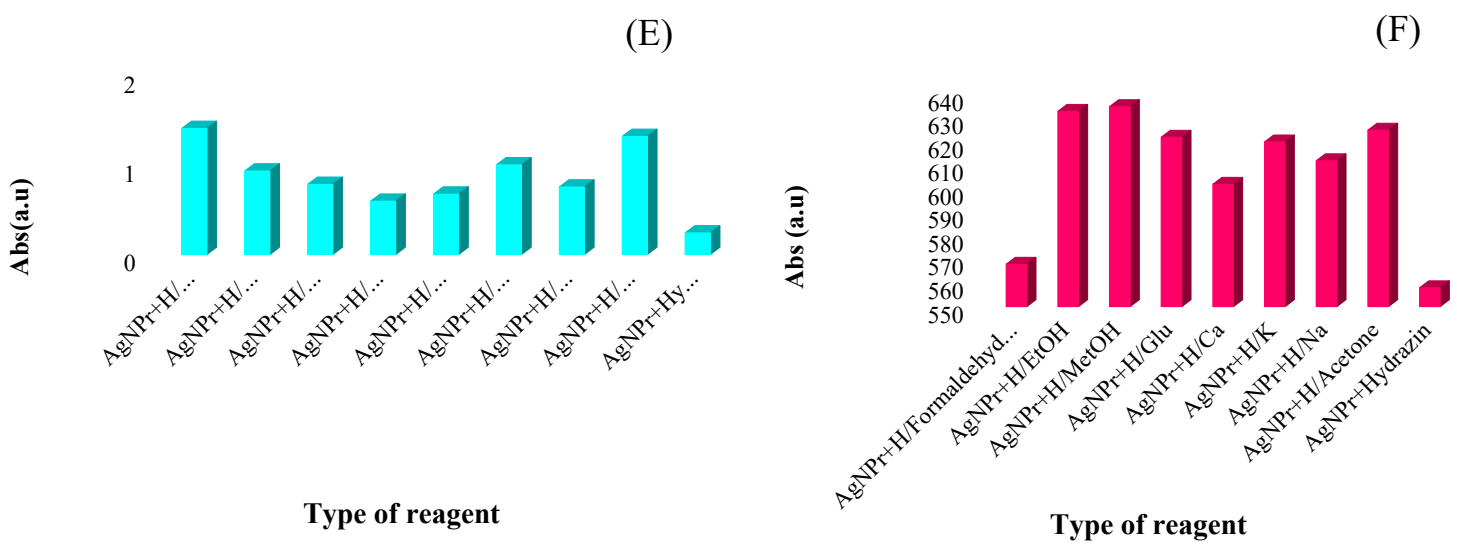


Fig. S12. **A, C)** UV-Vis spectra of different concentrations of Hyd in the presence of optical probes (AgNPs, AgNWs), respectively. **B, D)** Dependency of reaction time versus different concentrations of Hyd







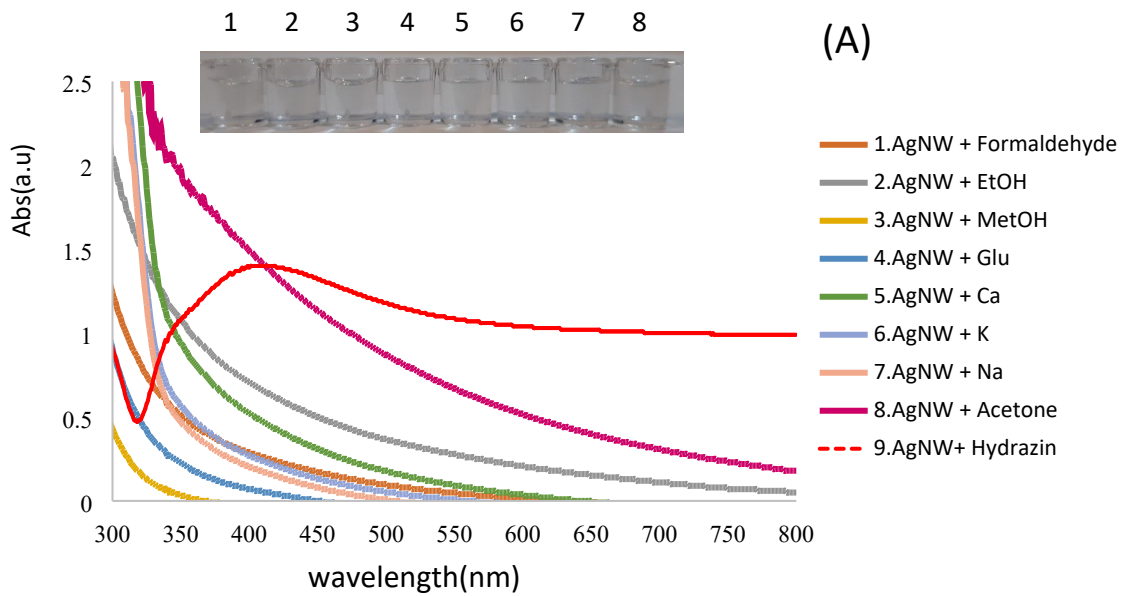


Fig. S13. photographic images and spectroscopic UV-Vis graphs of: **A)** AgNPr/Formaldehyde, AgNPr/EtOH, AgNPr/MetOH, AgNPr/Glu, AgNPr/Ca, AgNPr/K, AgNPr/Na, AgNPr/Acetone. **D)** AgNPr/(Formaldehyde+H), AgNPr/(EtOH+H), AgNPr/(MetOH+H), AgNPr/ (Glu+H), AgNPr/(Ca+H), AgNPr/(K+H), AgNPr/(Na+H), AgNPr/(Acetone+H). **B, E)** UV-Vis absorption response versus type of reagents. **C, F)** histogram of wavelength changes versus type of reagents.

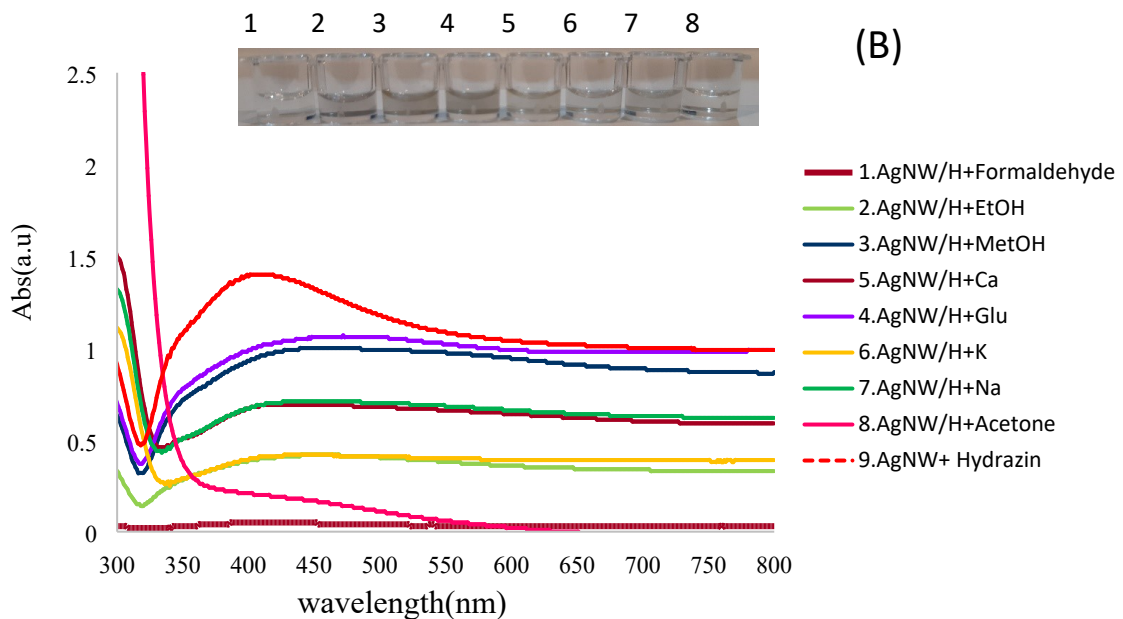


Fig. S14. photographic images and Spectroscopic UV-Vis graph of: **A)** AgNWs/Formaldehyde, AgNWs/EtOH, AgNWs/MetOH, AgNWs/Glu, AgNWs/Ca, AgNWs/K, AgNWs/Na, AgNWs/Acetone. **B)** AgNWs/(Formaldehyde+Hyd), AgNWs/(EtOH+ Hyd), AgNWs/(MetOH+ Hyd), AgNWs/(Glu+ Hyd), AgNWs/(Ca+ Hyd), AgNWs/(K+ Hyd), AgNWs/(Na+ Hyd), AgNWs/(Acetone+ Hyd).

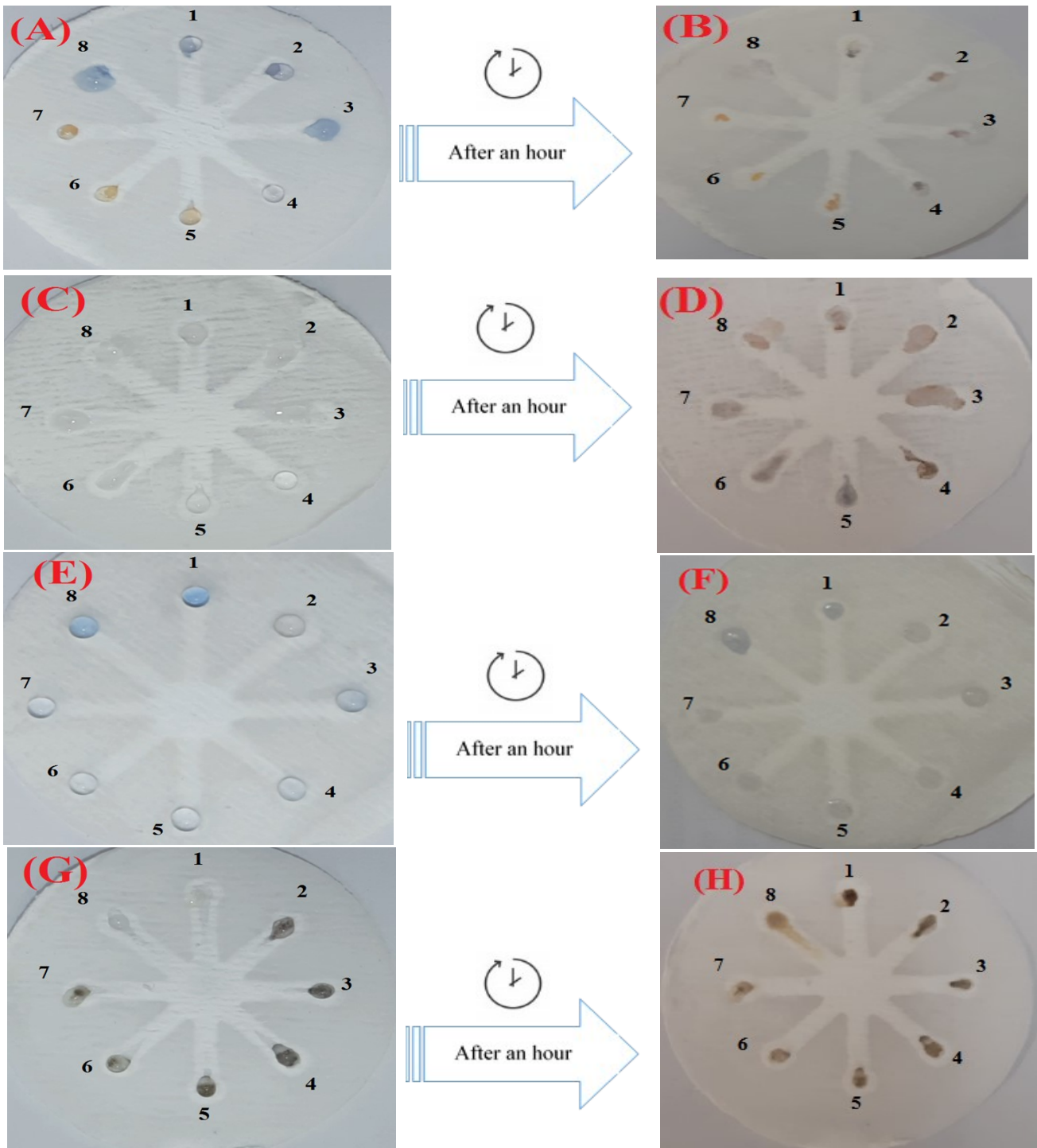
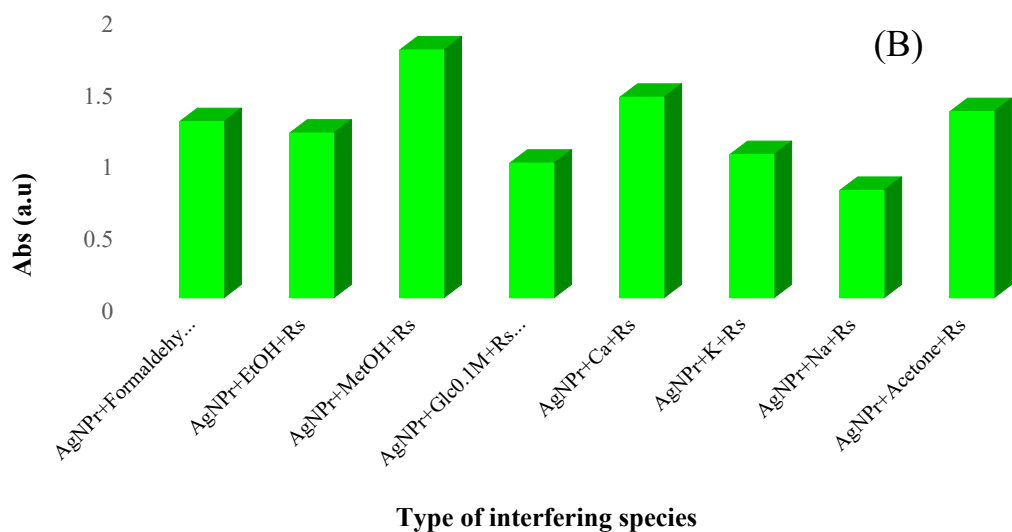
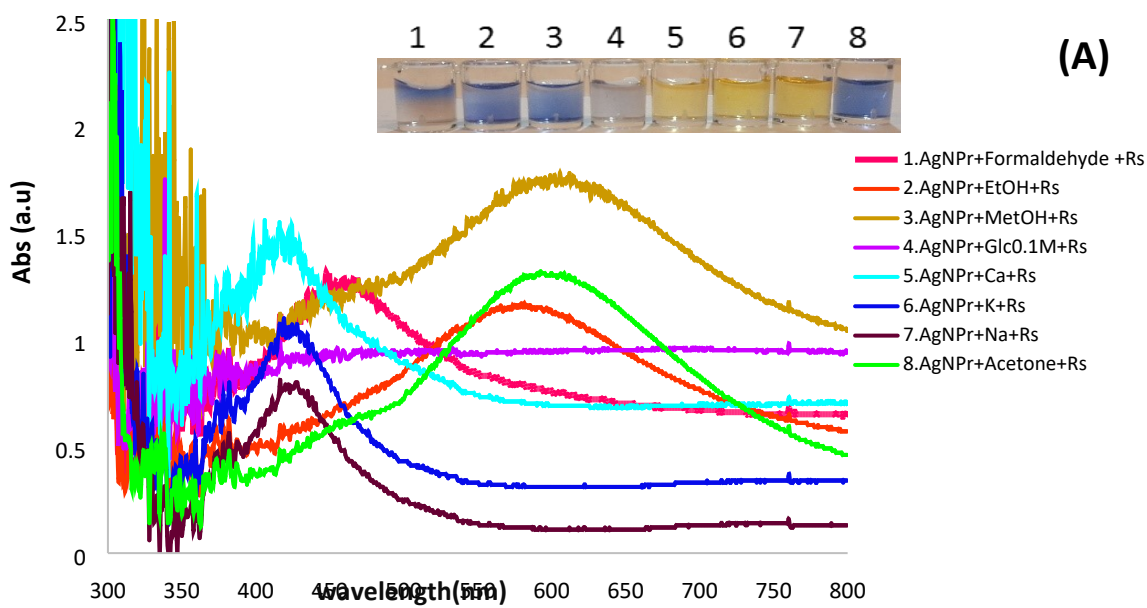
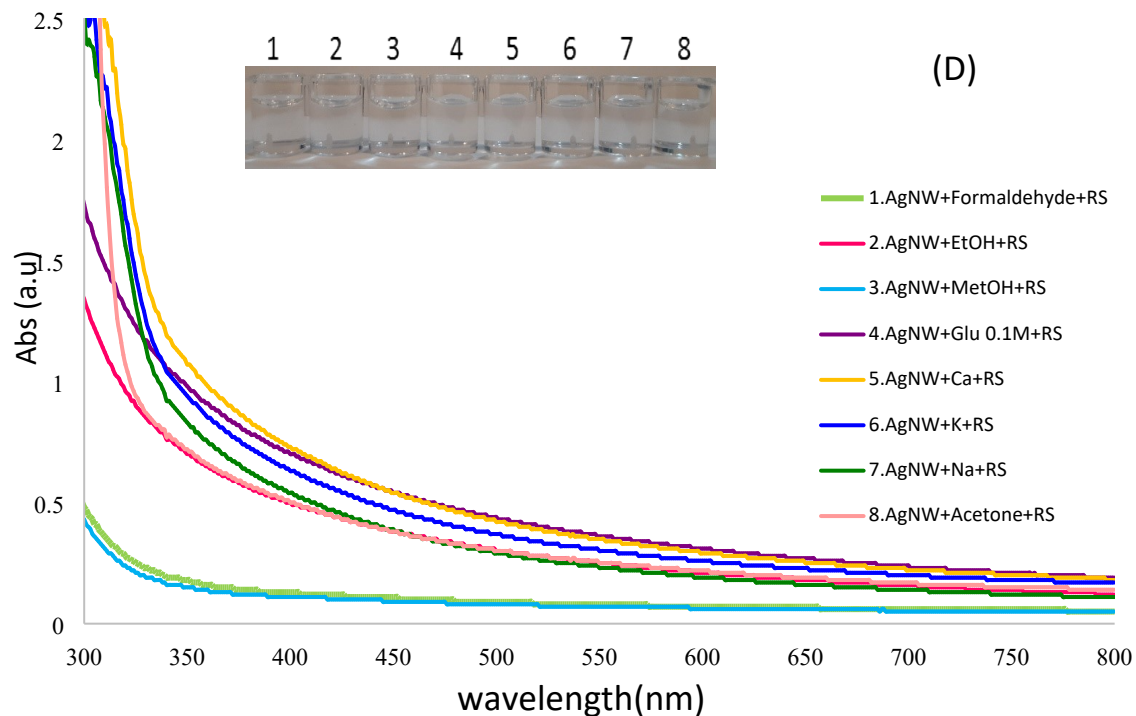
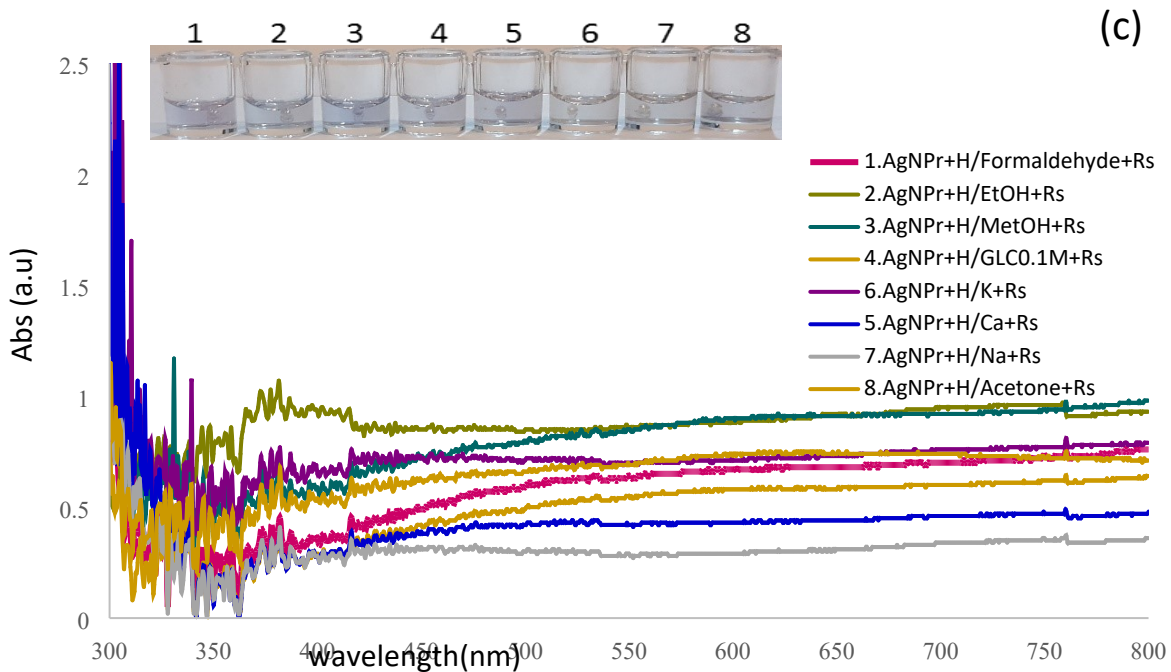


Fig. S15. Photographic images of the μ PCD-based calorimetric sensor: **A, D)** Interaction between AgNPs and AgNWs with (Formaldehyde, EtOH, MetOH, Glu, Ca, K, Na, and Acetone) zones 1 to 8, respectively before and after an hour. **C, G)** Interaction between AgNPs and AgNWs with (Formaldehyde+Hyd, EtOH+Hyd, MetOH+Hyd, Glu+Hyd, Ca+Hyd, K+ Hyd, Na+ Hyd, and Acetone+ Hyd) zones 1 to 8, respectively before and after an hour.





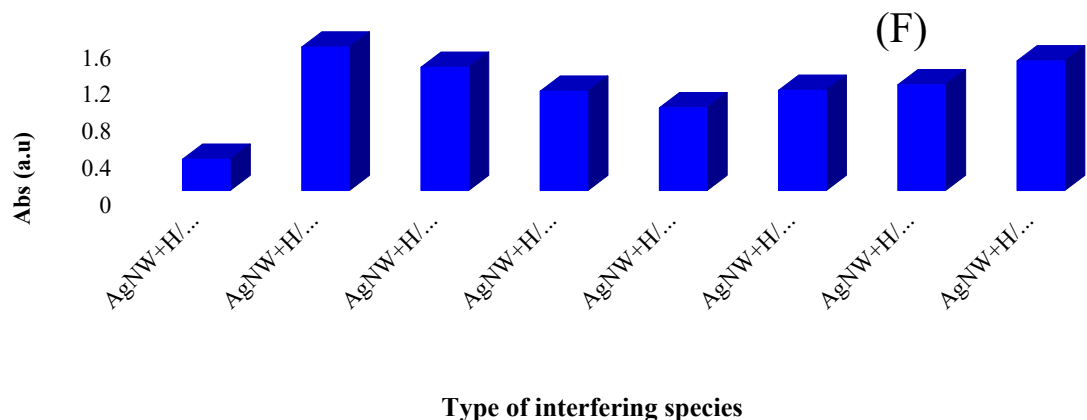
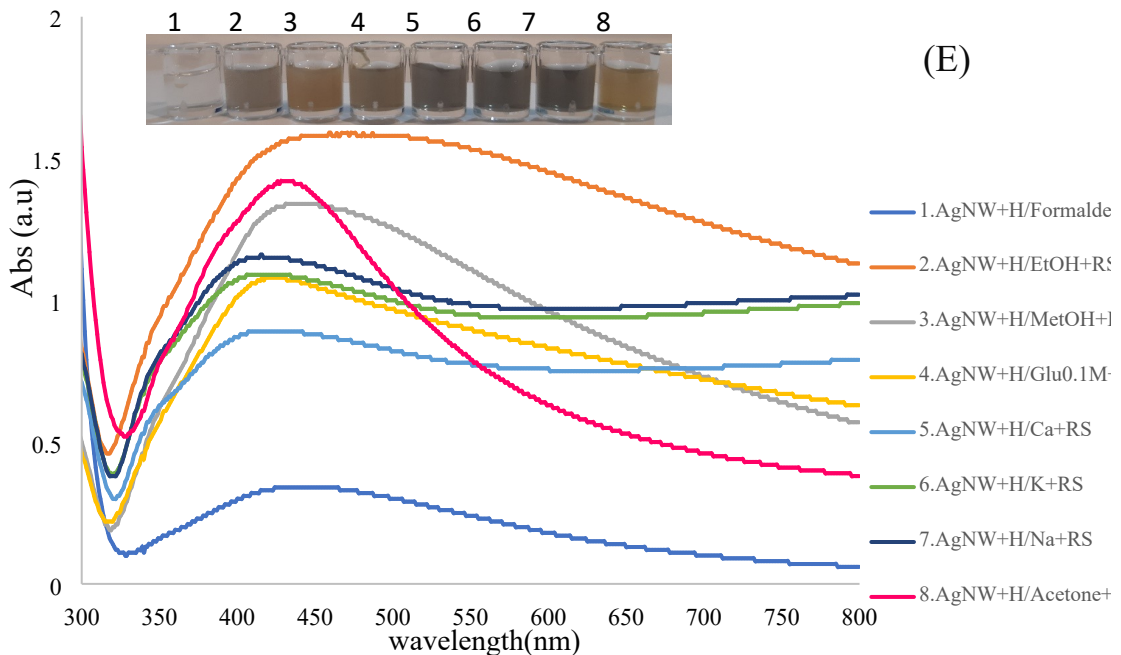
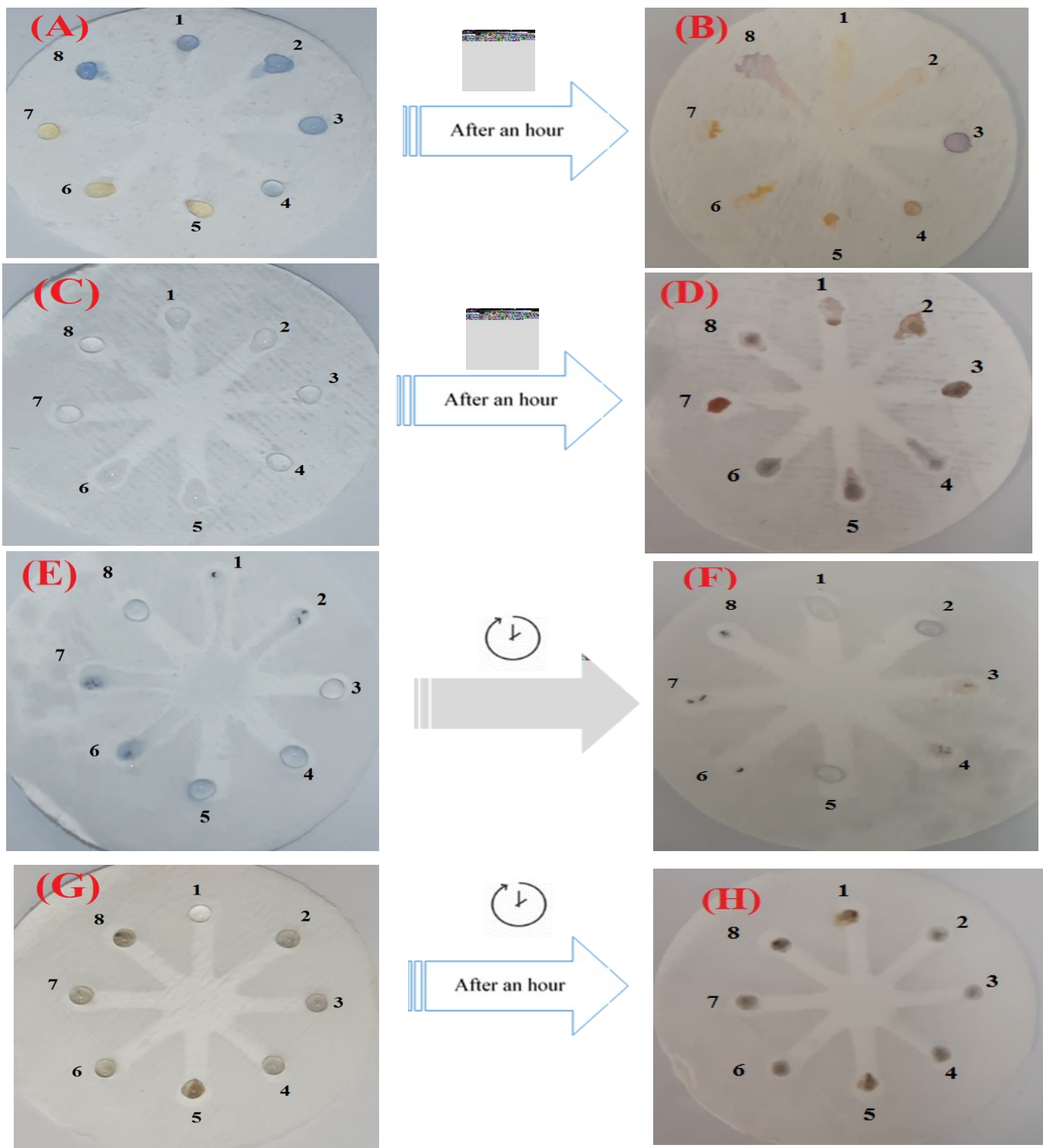


Fig. S16. photographic images and spectroscopic UV-Vis graphes of: **A)** AgNPr/Formaldehyde+Rs, AgNPr/EtOH+Rs, AgNPr/MetOH+Rs, AgNPr/Glu+Rs, AgNPr/Ca+Rs, AgNPr/K+Rs, AgNPr/Na+Rs, AgNPr/Acetone+Rs. **C)** AgNPr/(H/Formaldehyde+Rs), AgNPr/(H/EtOH+Rs), AgNPr/(H/MetOH+Rs), AgNPr/(H/Glu+Rs), AgNPr/(H/Ca+Rs), AgNPr/(H/K+Rs), AgNPr/(H/Na+Rs), AgNPr/(H/Acetone+Rs). **D)** AgNWs/Formaldehyde+Rs, AgNWs/EtOH+Rs, AgNWs /MetOH+Rs, AgNWs/Glu+Rs, AgNWs/Ca+Rs, AgNWs/K+Rs, AgNWs/Na+Rs, AgNWs/Acetone+Rs. **E)** AgNWs/(H/Formaldehyde+Rs), AgNWs/(H/EtOH+Rs), AgNWs/(H/MetOH+Rs), AgNWs/(H/Glu+Rs), AgNWs/(H/Ca+Rs), AgNWs/(H/K+Rs), AgNWs/(H/Na+Rs), AgNWs/(H/Acetone+Rs). **B, F)** UV-Vis absorption response versus type of reagents.

Fig. S17. Photographic images of the μ PCD-based calorimetric sensor: **A, D)** Interaction between AgNPs and AgNWs with (Formaldehyde/Rs, EtOH/Rs, MetOH/Rs, Glu/Rs, Ca/Rs, K/Rs, Na/Rs, and Acetone/Rs) zones 1 to 8, respectively before and after an hour. **C, G)** Interaction between AgNPs and AgNWs with (Formaldehyde/Rs+H, EtOH/Rs+H, MetOH/Rs+ Hyd, Glu/Rs+Hyd, Ca/Rs+ Hyd, K/Rs+ Hyd, Na/Rs+ Hyd, and Acetone/Rs+ Hyd) zones 1 to 8, respectively before and after an hour.



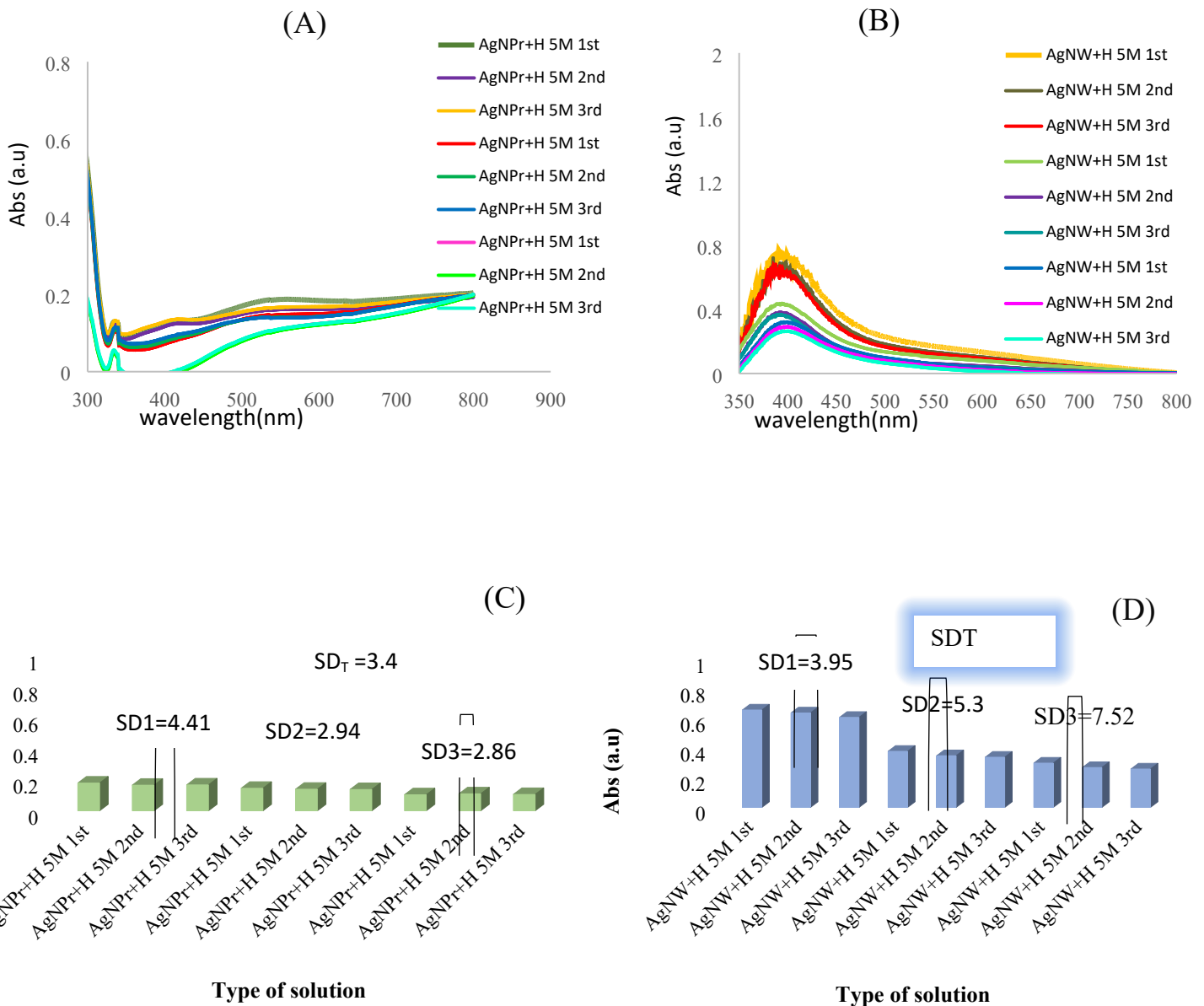


Fig. S18. Spectroscopic UV-Vis graphs record of the interaction of: **A)** AgNPrs **B)** AgNWs with 5M Hyd with three repeats, respectively; **C, D)** Histogram of Abs (A.u) *versus* type of solution.

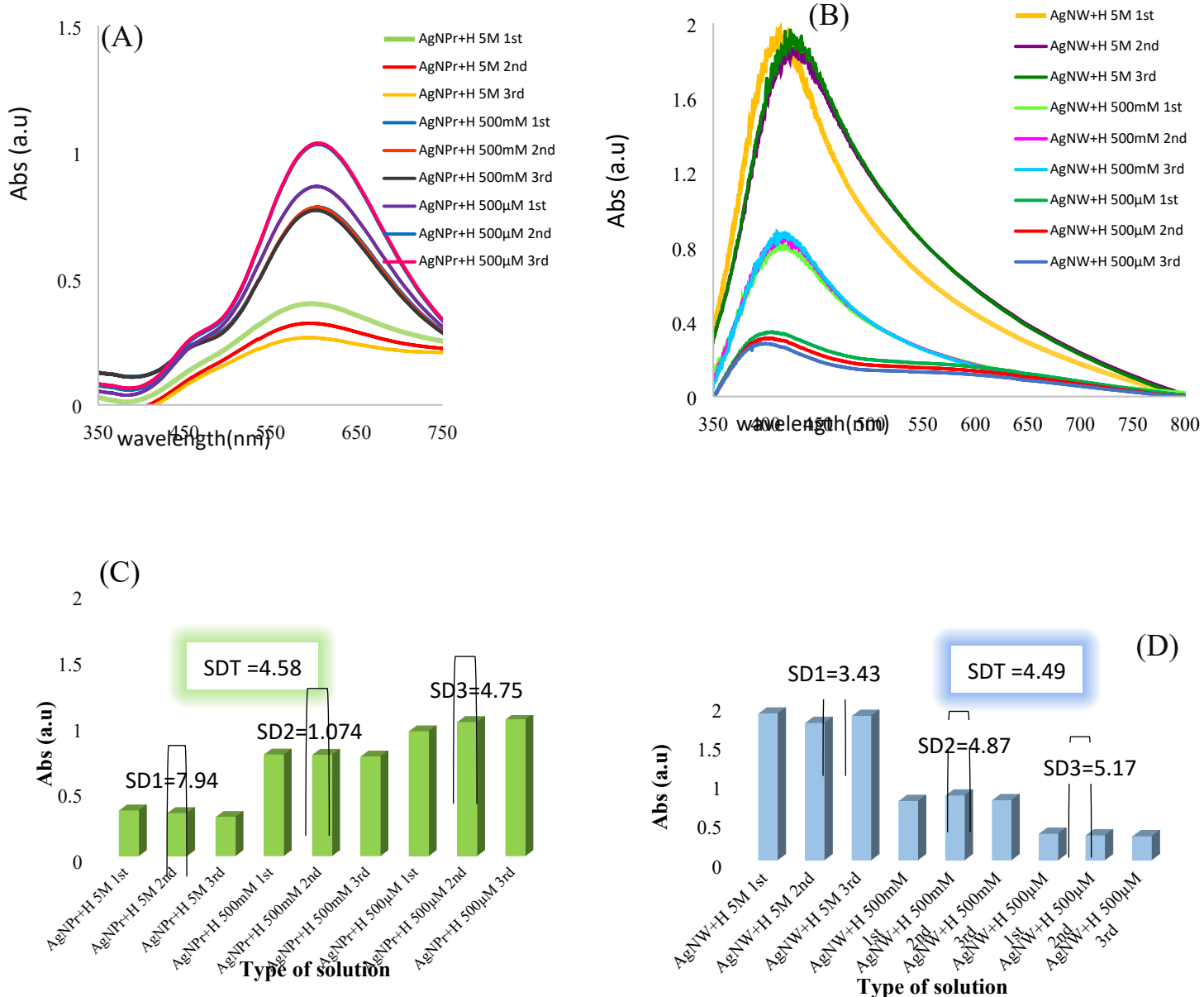
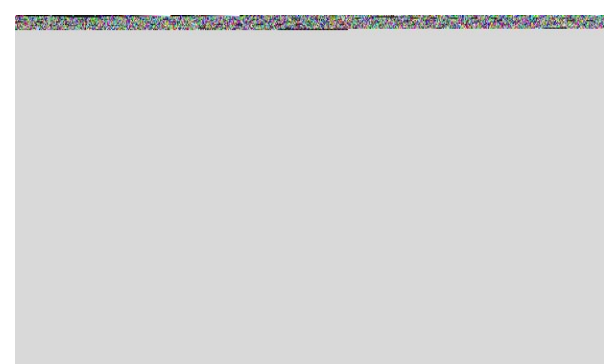
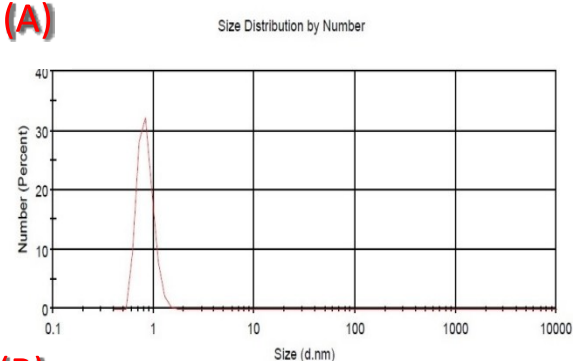


Fig. S19. Spectroscopic record of the interaction of: **A)** AgNPs, **B)** AgNWs with various concentrations of Hyd (5M, 500mM, 500μM); **C, D)** the absorbance of the reaction (A and B) in three repeats at the different concentrations, respectively.

(A)



(B)

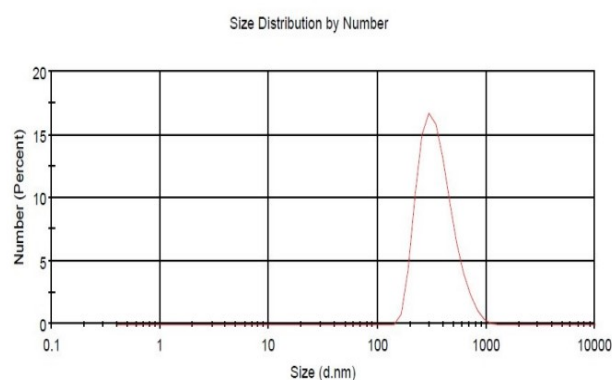
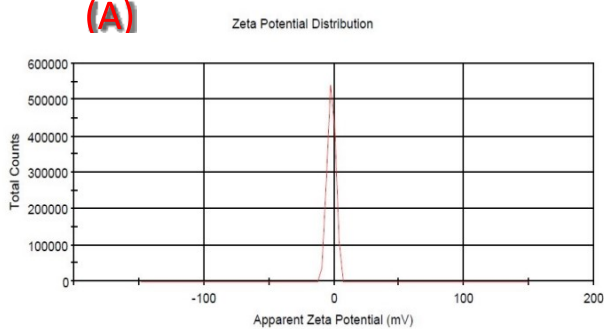


Fig. S20. DLS plots of A) Ag NPrs, B) AgNWs before and after 3 month.

(A)



(B)

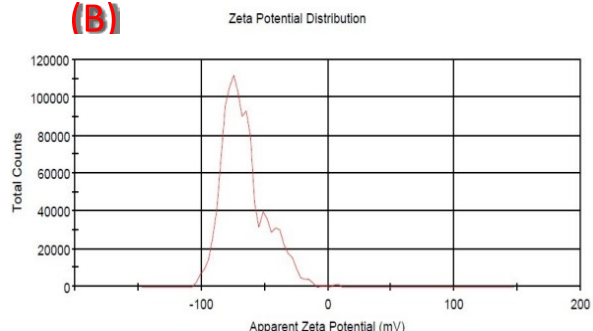


Fig. S21. Zeta potential of A) Ag NPrs, B) AgNWs before and after 3 months.

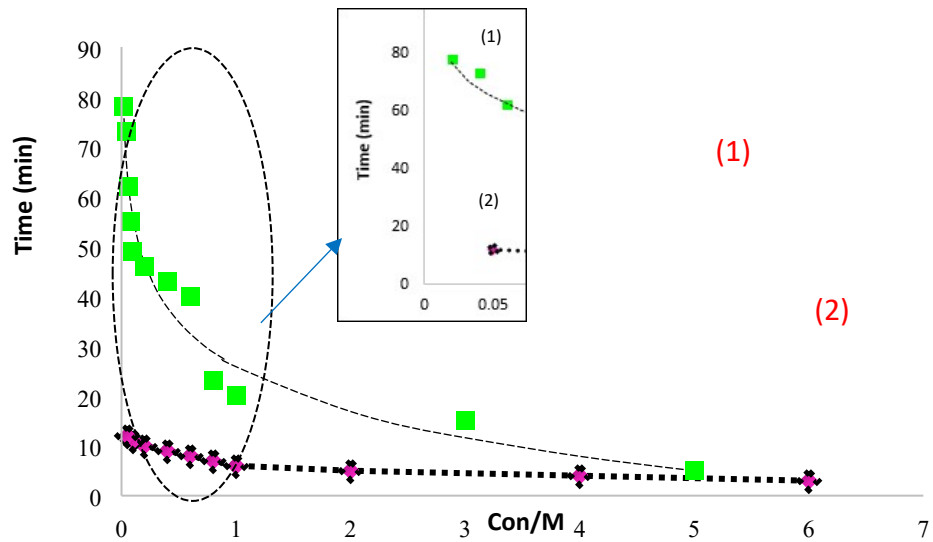


Fig. S22. Calibration curve of detection time versus different concentrations of Hyd in the presence of optical probes (1) AgNPrs and (2) AgNWs.